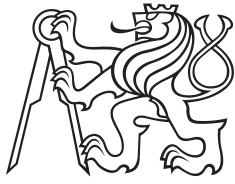


Bachelor Project



**Czech
Technical
University
in Prague**

F3

**Faculty of Electrical Engineering
Department of Radioelectronics**

Scattering of an Electromagnetic Wave by a Moving Highly-Conducting Object

Tomáš Duspiva

**Supervisor: Lukáš Jelínek
Field of study: Open Electronic Systems
May 2023**

I. Personal and study details

Student's name: **Duspiva Tomáš** Personal ID number: **499281**
Faculty / Institute: **Faculty of Electrical Engineering**
Department / Institute: **Department of Radioelectronics**
Study program: **Open Electronic Systems**

II. Bachelor's thesis details

Bachelor's thesis title in English:

Scattering of an Electromagnetic Wave by a Moving Highly-Conducting Object

Bachelor's thesis title in Czech:

Rozptyl elektromagnetické vlny na pohybujícím se dobře vodivém objektu

Guidelines:

Get acquainted with transforming an electromagnetic field into a co-moving frame of reference. Assuming uniform translation and objects made solely of highly-conducting materials, use an existing solver of Maxwell's equations in the co-moving frame based on the electric field integral equation. Prepare MATLAB packages that evaluate a scattered electromagnetic field from a generic incident electromagnetic field in the laboratory frame of reference. Apart from general and potentially computationally demanding package, prepare a computationally effective package for non-relativistic velocities.

Bibliography / sources:

- [1] C. Moller, The Theory of Relativity, Clarendon Press, 1955.
- [2] J. Bladel, Relativity and Engineering, Springer-Verlag, 1984.
- [3] B. L. Michielsen, G. C. Herman, A. T. de Hoop, and D. de Zutter, "Three-dimensional relativistic scattering of electromagnetic waves by an object in uniform translational motion", Journal of Mathematical Physics, Vol. 22, pp. 2716-2722, 1981.

Name and workplace of bachelor's thesis supervisor:

doc. Ing. Lukáš Jelínek, Ph.D. Department of Electromagnetic Field FEE

Name and workplace of second bachelor's thesis supervisor or consultant:

Date of bachelor's thesis assignment: **15.02.2023** Deadline for bachelor thesis submission: _____

Assignment valid until: **22.09.2024**

doc. Ing. Lukáš Jelínek, Ph.D.
Supervisor's signature

doc. Ing. Stanislav Vítek, Ph.D.
Head of department's signature

prof. Mgr. Petr Páta, Ph.D.
Dean's signature

III. Assignment receipt

The student acknowledges that the bachelor's thesis is an individual work. The student must produce his thesis without the assistance of others, with the exception of provided consultations. Within the bachelor's thesis, the author must state the names of consultants and include a list of references.

Date of assignment receipt

Student's signature

Acknowledgements

I would like to thank my supervisor for the feedback during my work and my family, my partner and my schoolmates for supporting me through the struggles.

Declaration

I declare that I completed the presented thesis independently and that all used sources are quoted in accordance with the Methodological instructions that cover the ethical principles for writing an academic thesis.

Prague, May 26, 2023

Prohlašuji, že jsem předloženou práci vypracoval samostatně a že jsem uvedl veškeré použité informační zdroje v souladu s Metodickým pokynem o dodržování etických principů při přípravě vysokoškolských závěrečných prací.

V Praze, 26. května 2023

Abstract

This thesis treats basic methodology to evaluate the scattering of electromagnetic field by a moving highly-conducting object. The solution is provided within the framework of special relativity using a frame-hopping technique. The electrodynamics is described by the electric field integral equation and method of moments. The thesis also covers the implementation in the MATLAB environment. The general treatment is compared to several approximative solutions to the same problem, such as low-speed approximation or point dipole approximation.

Keywords: radar, electromagnetic scattering, moving object, special relativity, method of moments, electric field integral equation, numerical solution

Supervisor: Lukáš Jelínek
Department of Electromagnetic Field,
Czech Technical University

Abstrakt

Tato práce se zabývá základními postupy výpočtu rozptylu elektromagnetického pole na pohybujícím se dobře vodivém objektu. Řešení využívá speciální teorii relativity a techniky frame-hopping. Elektrodynamika je popsána integrální rovnicí elektrického pole a metodou momentů. Práce se dále zabývá implementací řešení v prostředí MATLAB. Obecné řešení je porovnáváno s několika aproximativními řešeními stejného problému, jako je aproximace pro nízké rychlosti nebo bodová dipólová aproximace.

Klíčová slova: radar, rozptyl elektromagnetického pole, pohybující se objekt, speciální teorie relativity, metoda momentů, integrální rovnice elektrického pole, numerické řešení

Překlad názvu: Rozptyl elektromagnetické vlny na pohybujícím se dobře vodivém objektu

Contents

1 Introduction	1
1.1 Goals of the Thesis	2
1.2 Outline of the Thesis	2
2 Special relativity	5
2.1 Four-vectors and field tensor	6
2.1.1 Four-vectors	7
2.1.2 Field tensors	7
2.2 Lorentz transformation	7
2.3 Explicit transformation	8
2.4 Lorentz transform operator	9
3 Solution to Maxwell equations	11
3.1 Electric field integral equation	11
3.2 Galerkin method for EFIE	12
3.3 Implementation of Galerkin method	13
4 Implementation	15
4.1 General solution	15
4.1.1 Lorentz transformation of ω and full Lorentz transformation	16
4.1.2 Analytical full Lorentz transformation for a plane wave	18
4.1.3 Discretization of full Lorentz transformation	18
4.1.4 Full Lorentz transformation for dipoles	22
4.2 Implemented solution	23
5 Simplified test solutions	25
5.1 Dipole function	25
5.2 Low-speed approximation	26
6 Results	29
6.1 Electrically small perfectly conducting sphere	29
6.1.1 Program settings	29
6.1.2 Results for $v = 10^{-3}c$ and $v = 0.8c$	30
6.2 Thin-strip dipole discretized by 72 nodes	32
6.2.1 Program settings	32
6.2.2 Results for $v = 10^{-6}c$, $v = 10^{-4}c$ and $v = 10^{-3}c$	33
7 Conclusion	37
Bibliography	39

Figures

1.1 Parker Solar Probe.....	2
4.1 Color coding used in flowcharts.	15
4.2 Sketch of a solution to the problem of wave scattering by a moving object.	16
4.3 Flowchart corresponding to the transformation $\mathcal{L}[\mathbf{E}, \mathbf{B}, \mathbf{r}, \omega]$	17
4.4 Discretized version of the flowchart from figure 4.3.	19
4.5 Flowchart from figure 4.4 supplemented with interpolation ..	21
4.6 Flowchart of the final implemented solution.	23
5.1 Flowchart for a scattering from a polarizable dipole.	26
5.2 Approximation for low speed. ..	27
6.1 Discretized spherical surface consisting of 38 and 110 nodes. ...	30
6.2 $E_{sx}(t)$ and $ E_{sx}(\omega) $ of three different sphere descriptions for velocity $v = 10^{-3}c$	31
6.3 $E_{sx}(t)$ and $ E_{sx}(\omega) $ of three different sphere descriptions for velocity $v = 0.8c$	31
6.4 Mesh of a thin-strip dipole discretized by 72 nodes	32
6.5 $\log E_{sx}(\omega) $ of the main and the low-speed program for velocity $10^{-6}c$, $10^{-4}c$ and $10^{-3}c$	34

Tables

6.1 User input for the spherical setup	30
6.2 User input for the thin-strip dipole setup.....	33

Chapter 1

Introduction

Radar technology [1] experienced a long evolution since its battle premiere in the Second World War and its first publication [2] in the Nature journal. After the Second World War, this secret weapon evolved into a widely civil-used device and spread throughout the world. The radar had expanded its application from addressing speeding tickets over the physiology [3] to meteorology. Radar also became the natural tool for answering many questions in space exploration, giving rise to radar astronomy [4].

Skolnik [1] defines radar as: “*A radar operates by radiating electromagnetic energy and detecting the echo returned from reflecting objects (targets).*” The returned echo can be inspected in various ways. The directionality of the antenna can help to determine the direction of the object from the radar, the frequency shift, called Doppler shift, indicates the movement of the object and the velocity of the movement and, if the resolution of the radar is high enough, the information about the shape and size of the object can be obtained [5].

The above-mentioned definition of radar is rather broad. Nevertheless, radar is typically used in a narrower set of scenarios in which either the reflecting object is in the far field of the illuminating antenna, or the speed of the object is many orders in magnitude slower than the speed of light. Although these are the most practical cases, they are not the only ones. As an example, radar astronomy deals with objects such as asteroids (speed as high as 140000 km/h in our solar system), comets (speed as high as 250000 km/h in our solar system) or man-made probes, such as the Parker Solar Probe [6], which reaches speed as high as 700000 km/h. A different example is a radar mounted on an armoured vehicle which should track the path and properties of anti-tank missiles. In this case, the echoing objects must be tracked in the direct vicinity of the vehicle before they are destroyed.

In the last two cases, the radar detection is uneasy, and there is very little space for errors. These radar systems must therefore be thoroughly tested prior to their use. Since launching a test solar probe or fake missile is costly, these tests should be performed using synthetic data, i.e., data from numerical simulations. An important point in using synthetic data is also to see the limits of the approximations used in standard detection algorithms, where most commonly the non-relativistic Doppler effect and far-field approximation are used.

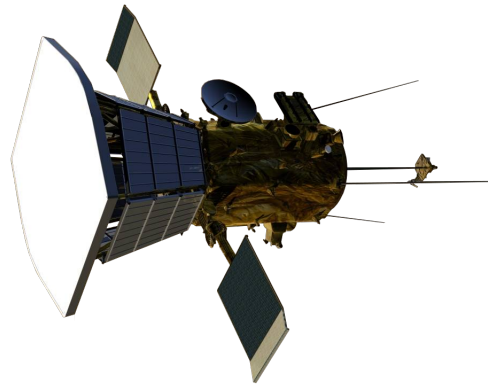


Figure 1.1: Parker Solar Probe.[6]

The previously described example demonstrates the practical application of a more theoretical problem, in which the electromagnetic waves produced by the known source scatter by an arbitrarily shaped object moving at an arbitrarily high fraction of the speed of light. A specific setup of this general electromagnetic problem is the main goal of this thesis.

The problem at hand has already been addressed by other authors. For example, an analytical solution to the scattering of a moving sphere in the plane wave field was given in [7, 8] or the usage of finite-difference time-domain (FDTD) method to solve scattering of the pyramid-shaped object was treated in [9]. A notable predecessor of this work is a recent paper [10] which uses integral equation formulation that is the most appropriate tool for scattering problems. This work will build upon this last work and aims at creating a freely available Matlab code that can be used by radar designers to generate synthetic testing data.

1.1 Goals of the Thesis

The primary goal of this thesis is to implement the scattering of an electromagnetic wave by a moving highly conducting object in general special-relativistic settings. The implementation should be compatible with the existing tool[11] for numerical solutions to Maxwell equations and should in the future be built in it as an external add-on in the Matlab environment. A secondary goal is to use the aforementioned general scenario to verify the correctness of low-speed approximations of this scattering problem.

1.2 Outline of the Thesis

In this work, the problem of scattering of the electromagnetic waves will be solved within the realm of special relativity, see chapter 2, using the frame-hopping technique [12]. In this framework, the incident wave is first transformed into the frame of the moving object. The scattering problem is

resolved within the object's rest frame using a standard method applicable to non-moving bodies, see chapter 3. The scattered field is afterwards transformed back into a laboratory frame. An important part of this thesis is the implementation of this scheme into the MATLAB environment, to which chapter 4 is devoted.

Chapter 2

Special relativity

About a century ago, Albert Einstein's *special and general relativity* introduced new insight into electrodynamics. The basic ingredient is the equivalence of all frames of reference and, therefore, the lack of need for any special coordinate systems to describe physics. This thesis will solely deal with special relativity, i.e., with inertial frames of reference. By this, the treatment presented here neglects the effects of acceleration on Maxwell's equations when the frame-hopping technique is used. In the rest frame of the body, here, Maxwell's equations are assumed to have the same form as in the inertial frame. From a practical standpoint, this assumption presents just a minor error, while computationally, the gain is high.

Special relativity is based on the following two postulates [12, 13]

- The laws of physics have the same form in all inertial frames.
- In an inertial frame, light always propagates in empty space with a definite speed c .

The relativity predecessor, non-relativistic Newtonian physics and the Galilean transformation hold only as an approximation for velocities small as compared to the speed of light [14].

The first postulate indicates that, when written correctly, the equations describing physics are identical in any inertial frame. The second postulate states that there exists a tool for changing the point of view of different frames. This tool is called is *Lorentz transformation*, detailed in section 2.2. There are several restrictive assumptions that make the problem at hand mathematically tractable. None of them is overly restrictive for describing problems connected to radar technology.

The major restrictions and approximations are:

- As a consequence of the second postulate, special relativity accepts only the non-accelerated movement. This assumption allows to use of simple field transformations when changing reference frames and, most importantly, allows to use of the standard form of Maxwell's equations in the rest frame of the moving object. This not only greatly simplifies their solution but also allows the use of already existing tools of computational electromagnetics.

- The trajectory of the object is predetermined and is not affected by the incident electromagnetic wave. This assumption presents almost no restriction with respect to macroscopic bodies, which are of interest to this work.

2.1 Four-vectors and field tensor

The proper formalism of relativity is the four-dimensional tensor algebra [12, 15], which is briefly introduced in this section for cases that are directly used in this work. In the case of electrodynamics, the essential components are four-vectors (position) and anti-symmetric tensors of second rank (electromagnetic field).

This formalism makes analytical calculations and thinking much easier, but computers cannot profit much from it. It is, therefore, a common practice to use three-dimensional formalism with transformation rules resulting from tensor algebra when implementing special relativistic calculations. In the case of the laboratory three-dimensional formalism is also typically used to report the experimental data.

In relativity, the indexing within tensors plays an important role and its position also defines the covariant (lower index) or the contravariant (upper index) of the physical object. The index-changing transformation tensor η_{ab} is called the *metric tensor*. Within special relativity, it stays the same in both cases, lowering and raising the indices [15]

$$\eta_{ab} = \eta^{ab} = \begin{pmatrix} 1 & 0 & 0 & 0 \\ 0 & -1 & 0 & 0 \\ 0 & 0 & -1 & 0 \\ 0 & 0 & 0 & -1 \end{pmatrix}. \quad (2.1)$$

A metric tensor is used to raise or lower the indices. For example, the Minkowski metric applied on a four-vector x^b

$$x^b = \begin{pmatrix} b_1 \\ b_2 \\ b_3 \\ b_4 \end{pmatrix} \quad (2.2)$$

reads [15]

$$x_a = \eta_{ab} x^b. \quad (2.3)$$

The result is

$$x_a = \begin{pmatrix} b_1 \\ -b_2 \\ -b_3 \\ -b_4 \end{pmatrix}. \quad (2.4)$$

2.1.1 Four-vectors

The position vector \mathbf{r} connects with the time t as the fourth coordinate to create the *position four-vector*

$$X^a = \begin{pmatrix} ct \\ r_x \\ r_y \\ r_z \end{pmatrix} = \begin{pmatrix} ct \\ \mathbf{r} \end{pmatrix}. \quad (2.5)$$

For unit consistency, the time is scaled by the speed of light c [15].

2.1.2 Field tensors

Within relativity, vacuum electromagnetic field is described by anti-symmetric *field tensor*

$$N_{mn} = \begin{pmatrix} 0 & -E_x/c & -E_y/c & -E_z/c \\ E_x/c & 0 & B_z & -B_y \\ E_y/c & -B_z & 0 & B_x \\ E_z/c & B_y & -B_x & 0 \end{pmatrix}. \quad (2.6)$$

The field tensor is an example of a two-dimensional tensor, therefore its element is described by two indices. Again, an electric field is divided by c for unit consistency [12, 15].

2.2 Lorentz transformation

The main advantage of tensor formalism is the ability of frame hopping, as the change of the frame of reference (“point of view”) is called. The choice of the correct reference frame can significantly simplify the calculations. A rest frame of the moving object, which will be used in this thesis, is one of these frames.

Conversion of quantities from one inertial frame (frame moving with constant velocity) to a different inertial frame is provided by *Lorentz transformation*. Lorentz transformation is described by tensor L_a^n . A common type of transformation used in this text is that of a tensor F_{mn} in a laboratory to a rest frame of a moving body in which it is denoted as F'_{mn} . The transformation reads

$$F'_{ab} = L_a^n L_b^m F_{nm}, \quad (2.7)$$

Now the *Lorentz transformation tensor* can be constructed as [12, 15]

$$L_a^n = \begin{pmatrix} \gamma & -\gamma \frac{v_x}{c} & -\gamma \frac{v_y}{c} & -\gamma \frac{v_z}{c} \\ -\gamma \frac{v_x}{c} & 1 + (\gamma - 1) \frac{v_x^2}{v^2} & (\gamma - 1) \frac{v_x v_y}{v^2} & (\gamma - 1) \frac{v_x v_z}{v^2} \\ -\gamma \frac{v_y}{c} & (\gamma - 1) \frac{v_y v_x}{v^2} & 1 + (\gamma - 1) \frac{v_y^2}{v^2} & (\gamma - 1) \frac{v_y v_z}{v^2} \\ -\gamma \frac{v_z}{c} & (\gamma - 1) \frac{v_z v_x}{v^2} & (\gamma - 1) \frac{v_z v_y}{v^2} & 1 + (\gamma - 1) \frac{v_z^2}{v^2} \end{pmatrix}, \quad (2.8)$$

where the normalized speed β in units of speed of light is defined as

$$\beta = v/c < 1 \quad (2.9)$$

and *Lorentz factor* γ as

$$\gamma(\beta) = \frac{1}{\sqrt{1 - \beta^2}} \geq 1. \quad (2.10)$$

The above relation can also be written using standard matrix algebra as

$$\mathbf{F}' = \mathbf{L}\mathbf{F}\mathbf{L}^T = \mathbf{L}\mathbf{F}\mathbf{L} \quad (2.11)$$

since tensor (matrix) \mathbf{L} is symmetric.

The application of Lorentz transformation to four-vector results in

$$x'^a = L_n^a x^n \quad (2.12)$$

or, if it is rewritten in matrix universum, in

$$\mathbf{x}' = \mathbf{L}\mathbf{x}. \quad (2.13)$$

The *inverse Lorentz transformation* [12] can be defined as a tool which returns the observer back to the original inertial frame. It is characterized by tensor L_a^n , which should fulfill the analogical equation to (2.7), i.e.,

$$x^n = L_a^n x'^a. \quad (2.14)$$

Since transforming the vector there and back must result in the same vector, there is

$$x'^a = L_n^a L_m^n x'^m \quad (2.15)$$

and

$$L_n^a L_m^n = \delta_m^a, \quad (2.16)$$

where δ_γ^a is Kronecker delta, or, in matrix language, a four-dimensional identity matrix.

After further inspection of the Minkowski metric, it can be concluded the inverse Lorentz and Lorentz transform tensors differ (expectedly) only in the sign on the velocity \mathbf{v} , i.e.

$$\mathbf{L}^{-1} = \mathbf{L}(\mathbf{v} := -\mathbf{v}). \quad (2.17)$$

The substitution is a consequence of the reciprocity of inertial frames, the same as the observer and the observed. The interchangeability of a Lorentz transformation velocity argument is a key fact because all codes performing the Lorentz transformation are easily invertible only by adding a minus to the speed arguments.

■ 2.3 Explicit transformation

Following the general rules for transforming tensors, this section sets out the explicit equations for transforming three-dimensional field quantities and

vectors from one inertial frame to another. This is also the way, how the transformations are implemented in the Matlab package.

Transformation of the field tensor is separated from the transformation of coordinates, therefore the coordinates still remain in the laboratory frame. These two first transformations can be applied in both, the time and frequency domain, unchanged: [12]

$$\mathbf{E}' = \mathbf{E}_{\parallel} + \gamma(\mathbf{E}_{\perp} + \mathbf{v} \times \mathbf{B}) \quad (2.18)$$

$$\mathbf{B}' = \mathbf{B}_{\parallel} + \gamma\left(\mathbf{B}_{\perp} - \frac{\mathbf{v} \times \mathbf{E}}{c^2}\right). \quad (2.19)$$

The field transformations must be supplemented by the transformation of coordinates. The explicit transformations of coordinates read

$$ct' = \gamma\left(ct - \frac{\mathbf{v} \cdot \mathbf{r}}{c}\right) \quad (2.20)$$

$$\mathbf{r}' = \mathbf{r} + \mathbf{v} \left[\frac{\mathbf{r} \cdot \mathbf{v}}{v^2} (\gamma - 1) - \gamma \frac{ct}{c} \right]. \quad (2.21)$$

As stated above, the relations explicit transform from a laboratory frame to a frame moving with velocity \mathbf{v} . The inverse transformations are obtained by reversing the direction of the velocity. This allows the implementation of only one such function in Matlab codes and, if the inverse transformation is needed, the same function is called with a different argument.

2.4 Lorentz transform operator

For easier notation in the following chapters, the *Lorentz transform operator* $\mathcal{L}[\cdot]$ is established, as the linear operator over previously mentioned pairs of physical quantities. The quantities will be paired as they occurred together in the four-vectors and the tensors in section 2.1. Operator $\mathcal{L}[\cdot]$ provides transformation

$$a', b' = \mathcal{L}[a, b] \quad (2.22)$$

of variables a, b , which are scalar or vector, in brackets to their corresponding images a', b' in the co-moving frame. Transformations are based on section 2.3. For example, applying operator on a pair \mathbf{r}, t , using (2.20) and (2.21), leads to

$$\mathcal{L}[\mathbf{r}, t] = \mathbf{r} + \mathbf{v} \left[\frac{\mathbf{r} \cdot \mathbf{v}}{v^2} (\gamma - 1) - \gamma t \right], \gamma \left(t - \frac{\mathbf{v} \cdot \mathbf{r}}{c^2} \right) = \mathbf{r}', t'. \quad (2.23)$$

Similarly, the *Inverse Lorentz transform operator* $\mathcal{L}^{-1}[\cdot]$ transforms the quantities back to the rest frame as

$$a, b = \mathcal{L}^{-1}[a', b'] \quad (2.24)$$

through the substitutions from section 2.3.

To ease the notation, the operators $\mathcal{L}[\cdot]$ and $\mathcal{L}^{-1}[\cdot]$ will also be used independently on multiple variables. Some of the quantities can be excluded from the transformation, the ones which are transformed are written out in subscripts, the example being

$$\mathcal{L}_{a,b}[a, b, c, d] = \mathcal{L}[a, b], c, d = a', b', c, d \quad (2.25)$$

This holds similar for the inverse Lorentz transform operator.

$$\mathcal{L}_{a',b'}^{-1}[a', b', c', d'] = \mathcal{L}^{-1}[a', b'], c', d' = a, b, c', d' \quad (2.26)$$

Applying the operators on functions f, g does not affect the argument of the functions, i.e.,

$$\mathcal{L}_{f,g}[f(a, b), g(a, b)] = f'(a, b), g'(a, b) \quad (2.27)$$

On the other hand, the operators can also be applied specifically only to the functions' argument, which does not change the functions¹ themselves.

$$\mathcal{L}_{a,b}[f(a, b), g(a, b)] = f(a(a', b'), b(a', b')), g(a(a', b'), b(a', b')) \sim f(a', b'), g(a', b') \quad (2.28)$$

For example, the coordinates-transformed fields stay as

$$\mathcal{L}_{r,t}[\mathbf{E}(\mathbf{r}, t), \mathbf{E}(\mathbf{r}, t)] = \mathbf{E}(\mathbf{r}(\mathbf{r}', t'), t(\mathbf{r}', t')), \mathbf{B}(\mathbf{r}(\mathbf{r}', t'), t(\mathbf{r}', t')) \sim \mathbf{E}(\mathbf{r}', t'), \mathbf{B}(\mathbf{r}', t'). \quad (2.29)$$

¹Actually, it does affect the functions, but just in a way that the new argument is first of all inserted in the substitution and after that, the whole functions are evaluated.

Chapter 3

Solution to Maxwell equations

Finding the scattering by an object means finding the solution to Maxwell equations. In this work, the solution will be performed in the rest frame of the object by which the incident field is scattered. The solution is provided using the electric field integral equation, which is the most appropriate tool for this scenario. Due to the operation within the rest frame, no change is needed to the standard procedure described below. The solution operates in the frequency domain, therefore, ω is omitted from the function arguments.

3.1 Electric field integral equation

Assuming that the known incident field $\mathbf{E}_i(\mathbf{r})$ exists in the rest frame of a general metal-dielectric object, the scattered electric field can be written as [16]

$$\mathbf{E}_s(\mathbf{r}) = -j\omega\mu \int_V \mathbf{G}(\mathbf{r}, \mathbf{r}_1) \cdot \mathbf{J}(\mathbf{r}_1) dV_1, \quad (3.1)$$

where

$$\mathbf{G}(\mathbf{r}, \mathbf{r}_1) = \frac{1}{4\pi} \left[\mathbf{I} + \frac{\Delta\Delta}{k^2} \right] \frac{e^{-jk|\mathbf{r}-\mathbf{r}_1|}}{|\mathbf{r}-\mathbf{r}_1|} \quad (3.2)$$

and where \mathbf{J} is the unknown polarization current density representing the object, and k is the wavenumber. The interaction of the material body with the field can then be described as [17]

$$\rho\mathbf{J} = \mathbf{E}_i + \mathbf{E}_s(\mathbf{J}), \quad (3.3)$$

where ρ is the resistivity of the material. This material relation must be enforced with the volume of the scatterer and gives rise to a linear operator equation for unknown current density \mathbf{J} called the electric field integral equation (EFIE).

The solution to (3.3) is commonly approached using Galerkin method [17].

3.2 Galerkin method for EFIE

Galerkin method, also known as the method of moments, provides a solution to the inhomogeneous linear operator equation

$$\mathcal{M}(\mathbf{f}) = \mathbf{g}, \quad (3.4)$$

where \mathbf{g} is a known complex vector function (excitation), and complex vector function \mathbf{f} is to be determined (response) [17].

Let Ψ_n be a set of basis functions [17] in the domain of \mathcal{M} . Then unknown vector \mathbf{f} can be written as their linear combination

$$\mathbf{f} = \sum_n I_n \Psi_n, \quad (3.5)$$

where I_n are expansion coefficients. Due to linearity, the equation (3.4) now reads

$$\sum_n I_n \mathcal{M}(\Psi_n) = \mathbf{g}. \quad (3.6)$$

Let a reaction product $\langle \mathbf{f}, \mathbf{g} \rangle$ be defined as [17]

$$\langle \mathbf{f}, \mathbf{g} \rangle = \int_V \mathbf{f} \cdot \mathbf{g} dV_1. \quad (3.7)$$

Then equations (3.6) can be tested by vector functions Ψ_n as

$$\sum_n I_n \langle \Psi_n, \mathcal{M}(\Psi_n) \rangle = \langle \Psi_n, \mathbf{g} \rangle. \quad (3.8)$$

This transforms the original operator equation into a system of linear equations [17]

$$\mathbf{Z}\mathbf{I} = \mathbf{V}, \quad (3.9)$$

where

$$Z_{mn} = \langle \Psi_m, \mathcal{M}(\Psi_n) \rangle \quad (3.10)$$

is *generalized impedance matrix*, \mathbf{I} are *generalized currents* and

$$V_m = \langle \Psi_m, \mathbf{g} \rangle \quad (3.11)$$

are called *generalized voltages* [17]. The solution to the problem (3.4) is transformed into the solution to a system of linear equations.

For the particular case of EFIE, the components of impedance matrix \mathbf{Z} are evaluated as

$$Z_{mn} = \langle \Psi_m, \rho \Psi_n - \mathbf{E}_s(\Psi_n) \rangle, \quad (3.12)$$

while the components of excitation vector \mathbf{V} are evaluated as

$$V_m = \langle \Psi_m, \mathbf{E}_i \rangle. \quad (3.13)$$

■ 3.3 Implementation of Galerkin method

Implementation of the Galerkin method over the electric field integral equation is not a goal of this thesis. Therefore, the author used a pre-implemented package[11] for this task. The used solver operates with RWG basis functions Ψ_n . The RWG functions are linearly increasing functions [18] defined over a triangular mesh and are well suited to describe scattering from arbitrarily shaped surfaces. The basis function is attached to each doublet of adjacent triangles forming an overall piecewise linear approximation of the surface current density field.

Chapter 4

Implementation

This chapter deals with the implementation of the Lorentz transformation discussed in chapter 2 and with the solution to a problem as a whole. The final coding is made in Matlab 2023a. To simplify the reading, all implementation steps will be shown using flowcharts which are then followed in the actual codes. Note that all flowcharts use the same colour coding, see figure 4.1. The interpolation nodes are brown because it is a mix of green and orange colour which represents analytic-like functions made out of discrete data.

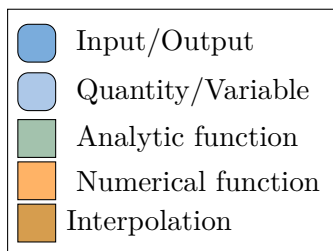


Figure 4.1: Color coding used in flowcharts.

4.1 General solution

In this section, a generic flowchart for the solved problem is given and thoroughly discussed. More specialized cases which are actually implemented are shown later on in section 4.2. The generic flowchart is shown¹ in figure 4.2.

¹The flowchart is inspired by a solution to a similar problem presented in [7].

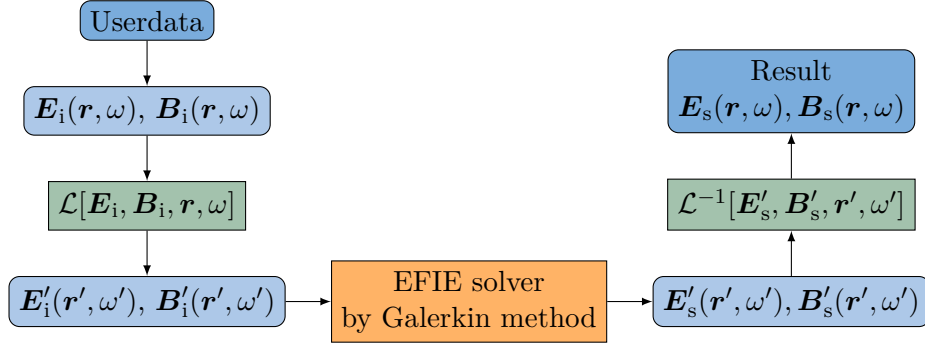


Figure 4.2: Sketch of a solution to the problem of wave scattering by a moving object.

Starting in the upper left corner, the user data are collected, and from this knowledge, the incident field within the laboratory frame \mathbf{E}_i and \mathbf{B}_i is evaluated. The incident field is assumed to be known in the frequency domain, which corresponds well with practice. Then the quantities are transformed in the co-moving frame via the Lorentz transformation, which will be explained further. Within the co-moving frame, the scattering problem with a static object is solved in the frequency domain using EFIE and Galerkin method. The solver generates scattered fields \mathbf{E}'_s and \mathbf{B}'_s , which are once more in the frequency domain. Now, the quantities are transformed back to the laboratory using inverse Lorentz transformation.

The major difficulty in performing the previous scheme lies in the two green transformations block. Notice, the operator $\mathcal{L}[\cdot]$ and $\mathcal{L}^{-1}[\cdot]$ are applied over ω or ω' , respectively, even though they were not defined for them before. Therefore, the green blocks must be studied in more detail. Since the two transformation blocks must only differ in the velocity direction, it is enough to study only one of them. The following development is, therefore, only related to the third block.

4.1.1 Lorentz transformation of ω and full Lorentz transformation

Assembling the third block, which will be named *full Lorentz transformation* further in the text, would carry out most of the requirements necessary for obtaining the scattered field because the block transforms everything involved from one frame to another.

Unfortunately, Lorentz transformations cannot be directly applied in frequency domain² since it connects only the space with time variables. The way to deal with this discomfort is to put the inverse Fourier transformation $\mathcal{F}_\omega^{-1}[\cdot]$ on the field variable to move from frequency domain ω to time domain t . Only then one can use the Lorentz transformation into the co-moving frame. After that, field quantities must be brought back to the frequency

²The frequency four-vector or four-frequency, on which could be the Lorentz transformation applied, does exist and is mostly used in optics, but it does not generally apply to this case [15].

domain (Fourier transform $\mathcal{F}_{t'}[.]$ into variable ω') since this is the domain of the electromagnetic solver. This 3-step way for the particular case of the electric field can be written as

$$\mathbf{E}(\mathbf{r}, t) = \mathcal{F}_{\omega}^{-1}[\mathbf{E}(\mathbf{r}, \omega)] \quad (4.1)$$

$$\mathbf{E}(\mathbf{r}', t') = \mathcal{L}_{\mathbf{r}, t}[\mathcal{F}_{\omega}^{-1}[\mathbf{E}(\mathbf{r}, \omega)]] \quad (4.2)$$

$$\mathbf{E}(\mathbf{r}', \omega') = \mathcal{F}_{t'}[\mathcal{L}_{\mathbf{r}, t}[\mathcal{F}_{\omega}^{-1}[\mathbf{E}(\mathbf{r}, \omega)]]], \quad (4.3)$$

where it is important to point out that the Fourier transformations in (4.3) are not inverses of each other, because they both operate in different frames.

The sum up to the flowchart corresponding to the left green block in 4.2, is shown in figure 4.3, where the linearity of the Fourier and Lorentz transformation was used, allowing move the Lorentz transformation block to the end of the flowchart.

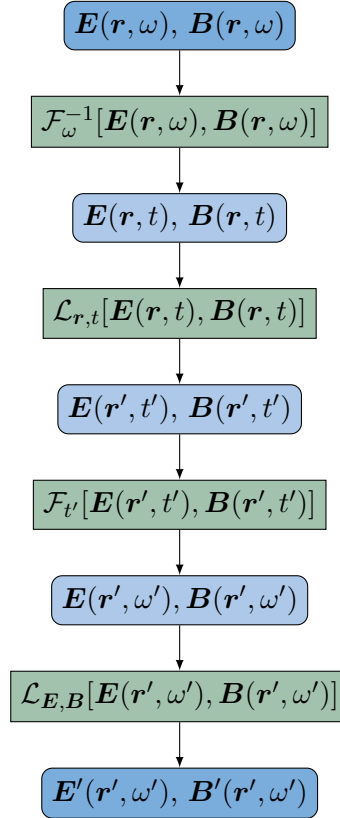


Figure 4.3: Flowchart corresponding to the transformation $\mathcal{L}[\mathbf{E}, \mathbf{B}, \mathbf{r}, \omega]$.

Particular examples of how to handle the full Lorentz transformation implementation-wise will be shown in the next subsections, discussing their strengths and weaknesses before the final implementation is presented.

4.1.2 Analytical full Lorentz transformation for a plane wave

The first method, allowing building up the components for the diagrams 4.2 and 4.3, consists of the assumption of canonical prescription of the electromagnetic field as a plane wave.

The electromagnetic field of a plane wave in the laboratory is defined as [16]

$$\mathbf{E}_{\text{PW}}(\mathbf{r}, \omega) = \mathbf{E}_0(\omega) e^{-j\frac{\omega}{c}\mathbf{n}\cdot\mathbf{r}} \quad (4.4)$$

and

$$\mathbf{B}_{\text{PW}}(\mathbf{r}, \omega) = \mathbf{B}_0(\omega) e^{-j\frac{\omega}{c}\mathbf{n}\cdot\mathbf{r}}, \quad (4.5)$$

where \mathbf{n} is a unit vector in the direction of plane wave propagation, $\mathbf{E}_0(\omega)$ is a field of a plane wave in origin and

$$\mathbf{B}_0(\omega) = \frac{1}{c}[\mathbf{n} \times \mathbf{E}_0(\omega)]. \quad (4.6)$$

In this case, the Full Lorentz transformation can be derived analytically as [12]

$$\mathbf{E}'_{\text{PW}}(\mathbf{r}', \omega') = \frac{1}{\gamma(1 - \beta\mathbf{n} \cdot \mathbf{v}_0)} \mathbf{E}'_0 \left(\frac{\omega'}{\gamma(1 - \beta\mathbf{n} \cdot \mathbf{v}_0)} \right) e^{-j\omega'\mathbf{n}'\cdot\mathbf{r}'} \quad (4.7)$$

$$\mathbf{B}'_{\text{PW}}(\mathbf{r}', \omega') = \frac{1}{\gamma(1 - \beta\mathbf{n} \cdot \mathbf{v}_0)} \mathbf{B}'_0 \left(\frac{\omega'}{\gamma(1 - \beta\mathbf{n} \cdot \mathbf{v}_0)} \right) e^{-j\omega'\mathbf{n}'\cdot\mathbf{r}'} \quad (4.8)$$

where

$$\mathbf{n}' = \frac{\mathbf{n} + [\mathbf{n} \cdot \mathbf{v}_0(\gamma - 1) - \gamma\beta] \mathbf{v}_0}{\gamma(1 - \beta\mathbf{n} \cdot \mathbf{v}_0)}. \quad (4.9)$$

and where $\mathbf{E}'_0, \mathbf{B}'_0$ relates to $\mathbf{E}_0, \mathbf{B}_0$ via (2.18) and (2.19).

An interesting property of a plane wave, seen from (4.7) and (4.8), is that it always remains a plane wave in any inertial frame. The only difference is an amplitude scaling, a stretched frequency axis, and a different propagation vector.

The solution for a plane wave is the simplest solution of all, its main advantage is the low computational complexity since the whole solution is analytical.

4.1.3 Discretization of full Lorentz transformation

A dangerous jump to a more complex and general solution of the full Lorentz transformation is to discretize the whole process. The discretization will lead to implementing the entire full Lorentz transformation in Matlab codes. Discretization is necessary, because limiting the code options to only few particular examples that can be solved analytically, is unwanted.

The Lorentz transformations from figure 4.3 will not be changed by discretization since they are written explicitly in analytical form. However, that does not apply to Fourier transformations, which must be replaced by Fast Fourier transform (FFT) [19].

Using the FFT and IFFT (inverse Fast Fourier Transform) leads to sampling the quantities. Asking the output function for a specifically sampled field in the co-moving frame pushes the frequency in the rest frame to be also sampled in a way that corresponds to its co-moving sibling. Therefore, the influence of choosing \mathbf{r}', ω' must be included in the input block, because the $\mathbf{E}'(\mathbf{r}', \omega')$ and $\mathbf{B}'(\mathbf{r}', \omega')$ cannot be obtained by reversing through the processes. Therefore the ω' and \mathbf{r}' transfer from the argument of the output function to the (\mathbf{r}, ω) argument of the input function. The transfer is done by estimation function, whose construction will be, for this moment, unspecified. The estimation step is a price for the discretization of the problem, and the ability to process any incident field.

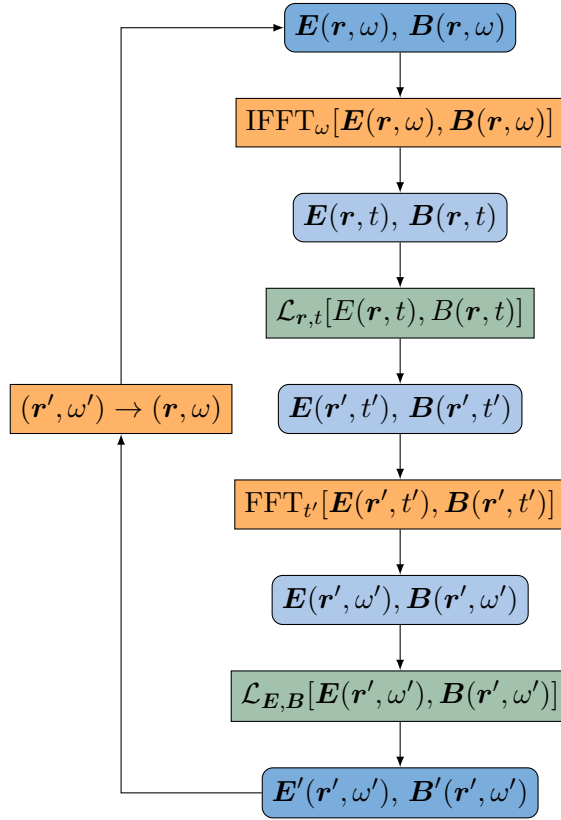


Figure 4.4: Discretized version of the flowchart from figure 4.3.

The discretization of the process makes some steps uncomfortable, especially the transition of the time coordinate from the laboratory to the co-moving frame. The FFT algorithm requires equidistant sampling and spectrum where positive frequency samples are complex conjugates of negative frequency samples, including a sample for $t = 0$ in the time domain or $\omega = 0$ in the frequency spectrum, with one sample added to the left side of the spectrum [19]. That sampling creates a straight beat in the time domain with corresponding frequency coordinates. It is necessary to hold the beat for proper work of the FFT algorithm.

On the other hand, the Lorentz transformation of the time variable generates

a time shift

$$ct' = \gamma \left(ct - \frac{\mathbf{v} \cdot \mathbf{r}}{c} \right), \quad (4.10)$$

see (2.20). The time shift can create off-beat samples, which are not matched with the condition of symmetric sampling. That results in FFT stopping working. In most cases, samples are not shifted by multiples of sampling periods. Hence, an appropriate deployed sampling in the laboratory rest frame does not guarantee proper sampling in the co-moving frame. Since the quantities between the sampling points are unknown, a few more blocks must be added to the scheme 4.4 for stabilization and symmetrization of sampling.

In this thesis, interpolation is used to estimate arbitrary function values between sampling points. Adding the two interpolations in two directions results in two separated coordinate set sequences, which would be the same coordinates in continuous space, but for discrete samples, they are not equal.

For limited computational memory, the user of the Matlab package is rather interested in interpolation over only one variable, not over the whole position four-vector. Luckily, the request can be fulfilled since the Lorentz transformation is used to simplify the position vector. Therefore, the position vector remains constant through the interpolation and the only variable varying through the interpolation is time. To make this assumption, the interpolation block must be placed, where the position of its argument is static.

The following three functions will be interpolated over t' in two blocks

$$\text{First interpolation block: } \begin{bmatrix} \mathbf{E}(\mathbf{r}', t') \\ \mathbf{B}(\mathbf{r}', t') \end{bmatrix} \quad (4.11)$$

$$\text{Second interpolation block: } \begin{bmatrix} \mathbf{r}(\mathbf{r}', t') \end{bmatrix}. \quad (4.12)$$

The previously mentioned two sets of coordinates sequence are distinguished by indices α, β . Borders between two areas of each index are the interpolations blocks.

The first block will be placed after the Lorentz transformation of coordinates allowing to match samples to FFT needs in a co-moving frame. As the assumption holds for \mathbf{r}' , which represents the state position of the object in the co-moving, therefore $\mathbf{r}_\alpha = \mathbf{r}_\beta$.

Concurrently with placing the second interpolation block, the mysterious block $(\mathbf{r}', \omega') \rightarrow (\mathbf{r}, \omega)$ is figured out.

Firstly the ω_α must be transformed in time t_β which has to satisfy[19]

$$N = \frac{2\pi}{\Delta t_\alpha \Delta \omega_\alpha}, \quad (4.13)$$

where the Δt_α and $\Delta \omega_\alpha$ is sampling step in the time, respectively frequency domain. Then it could be transformed into the laboratory frame and interpolated to satisfy laboratory IFFT requirements. Because ω_β in its freedom could break the Nyquist condition or put ω_β away under input sampling

requirements, therefore its estimation must be made.³ From ω_β is t_β received in analogical way as in (4.13).

After insertion of the interpolation blocks, the flowchart from figure 4.4 updates to figure 4.5.

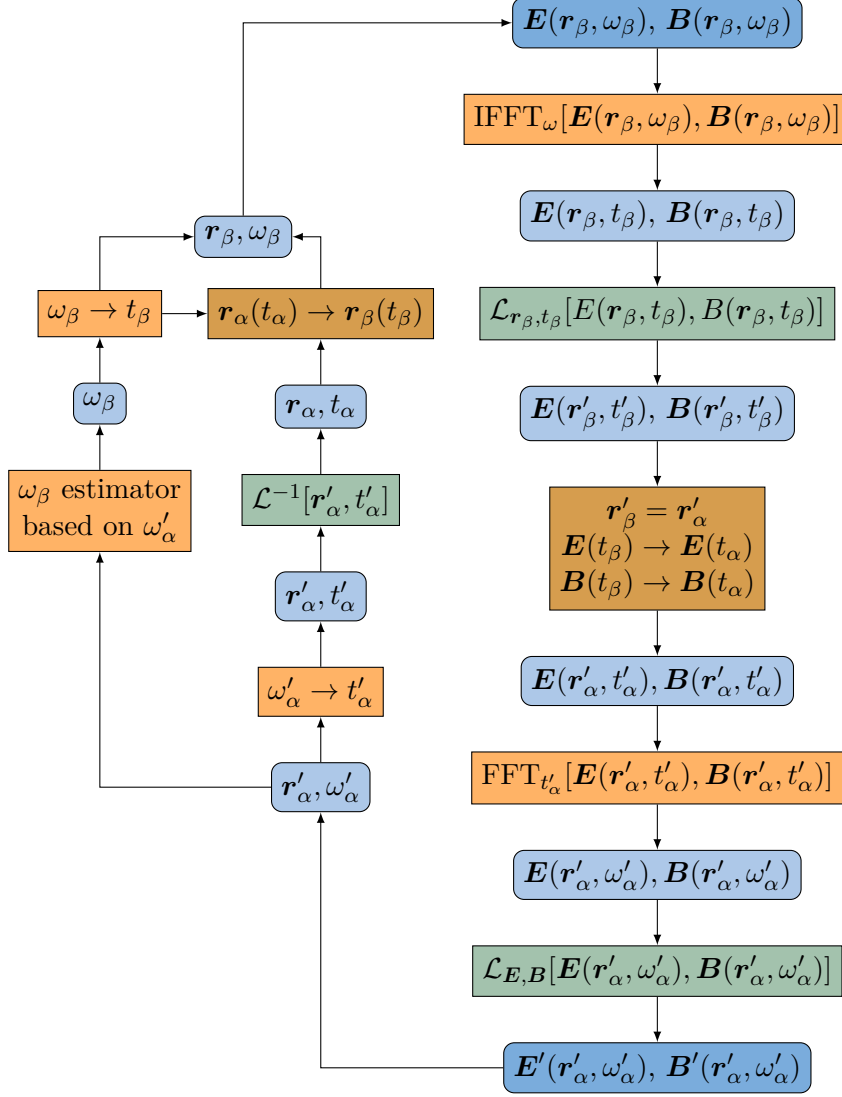


Figure 4.5: Flowchart from figure 4.4 supplemented with interpolation

The unexpected problem, which was not taken into account yet, is both interpolations are connected and they communicate with each other.

Interpolation of the position leads to extrapolation of the field and vice versa. The author wants to avoid extrapolation because he thinks extrapolation can produce enormous errors. Luckily, the transformation position (2.20) is linear respective to time⁴, ergo the analytic relationship can be obtained

³After a few failed attempts for proper estimation in code, the ω_β is estimated by a user for this moment.

⁴As expected, because the motion is uniform and linear.

through finite differences (gradient). In that case, the extrapolation is painless, because it does not have to be paid with an error. Therefore, the author chose to interpolate the fields and extrapolate the coordinates. This must be taken into account through the estimation of ω_β .

The issue of the solution in figure 4.5 hides in the IFFT block, because its output has to be one value for position at one time moment. Hence, the input calls for one full spectrum for each position, resulting in N calling for a unique N -element spectrum for each coordinate. The computational complexity grows over the number of samples, which arises in complicated manipulation with memory, and it will necessarily lead to the long execution time of the program. Therefore, the author abandoned these problems unsolved for this moment and suggested some solutions in the last chapter of this thesis 7. Fortunately, the solver output quantity has been forgotten until now, and it is time for it to step forward.

4.1.4 Full Lorentz transformation for dipoles

Since the outcome of the used EFIE solver is current density (smooth distribution of electric dipoles), one of the possibilities is to compose the scattered field from separate dipole responses. Using the dipole moment as the input quantity leads to another solution of full Lorentz transformation.

The electromagnetic fields of an electric dipole in a co-moving frame occur as[16]

$$\mathbf{E}'_{\text{E.dip}}(\mathbf{r}', t') = \frac{1}{4\pi\epsilon R'} \left(\frac{\mathbf{R}'_0 \times (\mathbf{R}'_0 \times \dot{\mathbf{p}}'_{\text{ret}})}{c^2} + \frac{[3\mathbf{R}'_0\mathbf{R}'_0 - \mathbf{I}] \cdot \dot{\mathbf{p}}'_{\text{ret}}}{R'c} + \frac{[3\mathbf{R}'_0\mathbf{R}'_0 - \mathbf{I}] \cdot \mathbf{p}'_{\text{ret}}}{R'^2} \right) \quad (4.14)$$

$$\mathbf{B}'_{\text{E.dip}}(\mathbf{r}', t') = -\frac{Z_0}{4\pi R'} \mathbf{R}'_0 \times \left(\frac{1}{c^2} \ddot{\mathbf{p}}'_{\text{ret}} + \frac{1}{R'c} \dot{\mathbf{p}}'_{\text{ret}} \right), \quad (4.15)$$

where \mathbf{p}'_{ret} denotes retarded time argument $\mathbf{p}'(t' - \frac{R'}{c})$, dots represent derivative with respect to the function argument, vector \mathbf{p}' stand for the electric dipole, and $\mathbf{R}' = \mathbf{r}' - \mathbf{r}'_{\text{dip}}$ with R' denoting distance $|\mathbf{R}'|$ and \mathbf{R}'_0 being unit vector along \mathbf{R}' . The final scattered field is the superposition of all dipoles describing the current density of the object.

Because the electromagnetic fields of dipoles can be analytically described in the time domain, the inverse Fourier transforms in 4.3 would be rather done over the dipole moment. This little switch between a field evaluation and the IFFT leads to a solution to the computational problem. Now, the information about solver quantity, this time the electric dipole, is requested only in one position per dipole because the object and, consequently, the dipoles are not moving in a co-moving frame. After the electric dipole in time is easily obtained through IFFT, the field can be calculated for the moving observer in the co-moving frame. That is truly easier because it

means calculating IFFT only few times, actually nine times per dipole (three for each coordinate times three for zeroth, first and second derivative), which is usually much less than the previous N times.

4.2 Implemented solution

As a summary of this chapter, the scheme shown in figure 4.6 will be implemented. The final solution is built from the solution of the full Lorentz transformation for plane wave as a source and from a set of electric dipoles representing the object scattering. The ω estimation has returned to its original block form from 4.4. This solution is used for numerical results in this thesis in chapter 6.

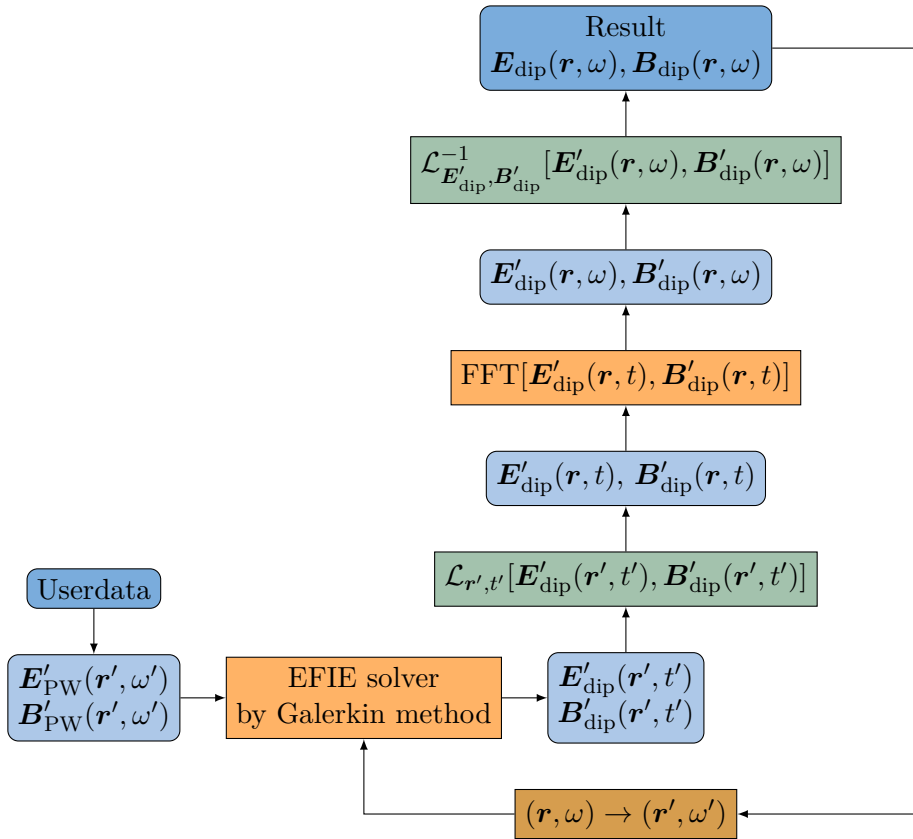


Figure 4.6: Flowchart of the final implemented solution.

Chapter 5

Simplified test solutions

In order to provide benchmarking and testing of the developed codes, simplified solutions of the same problem sketched in flowchart 4.2 are needed. This chapter is devoted to two such cases, one of which is a closed-form solution.

5.1 Dipole function

The first simplified solution consists of a laboratory plane-wave incident upon a moving non-dispersive (frequency-independent) polarizable dipole. The polarizable particle is described by its electric \mathbf{p} and magnetic \mathbf{m} dipole moment

$$\mathbf{p}'(\mathbf{r}', t') = \varepsilon_0 \alpha^e \mathbf{E}'_i(\mathbf{r}', t') \quad (5.1)$$

$$\mathbf{m}'(\mathbf{r}', t') = \frac{1}{\mu_0} \alpha^m \mathbf{B}'_i(\mathbf{r}', t'), \quad (5.2)$$

where α^e, α^m are non-dispersive electric and magnetic polarizabilities and ε_0 and μ_0 is permittivity and permeability of vacuum, respectively. For benchmarking purposes, polarizabilities of a perfectly conducting sphere $\alpha^e = 3V$, $\alpha^m = -3/2V$ are used with V being the volume of the sphere.

The time-domain electric and magnetic field of an electric dipole has already been introduced in (4.14) and (4.15). The fields created by magnetic dipole are dual and read [16]

$$\mathbf{E}'_{\text{M.dip}}(\mathbf{r}', t') = \frac{Z_0}{4\pi R'} \mathbf{R}'_0 \times \left(\frac{1}{c^2} \ddot{\mathbf{m}}'_{\text{ret}} + \frac{1}{R'c} \dot{\mathbf{m}}'_{\text{ret}} \right) \quad (5.3)$$

$$\mathbf{B}'_{\text{M.dip}}(\mathbf{r}', t') = \frac{\mu}{4\pi R'} \left(\frac{\mathbf{R}'_0 \times (\mathbf{R}'_0 \times \ddot{\mathbf{m}}'_{\text{ret}})}{c^2} + \frac{[3\mathbf{R}'_0 \mathbf{R}'_0 - \mathbf{I}] \cdot \dot{\mathbf{m}}'_{\text{ret}}}{R'c} + \frac{[3\mathbf{R}'_0 \mathbf{R}'_0 - \mathbf{I}] \cdot \mathbf{m}'_{\text{ret}}}{R'^2} \right). \quad (5.4)$$

The final scattered field is a superposition of both contributions

$$\mathbf{E}'_s = \mathbf{E}'_{\text{dip}} = \mathbf{E}'_{\text{E.dip}} + \mathbf{E}'_{\text{M.dip}} \quad (5.5)$$

$$\mathbf{B}'_s = \mathbf{B}'_{\text{dip}} = \mathbf{B}'_{\text{E.dip}} + \mathbf{B}'_{\text{M.dip}}. \quad (5.6)$$

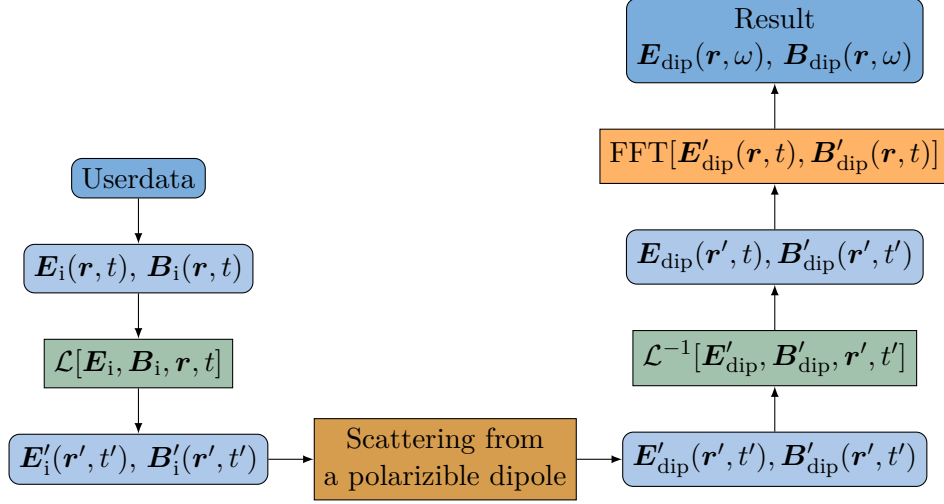


Figure 5.1: Flowchart for a scattering from a polarizable dipole.

Since the plane wave has an analytical representation in the time domain, the time characterization is taken as a solver in this case. The whole process sketched in flowchart 5.1 is mostly analytical, with the only exception of the final Fourier transforms and time derivatives that are needed in relations (5.3) and (5.4). These two numerical pieces are provided by FFT and finite differences. The purpose of this solution is to check the validity of the main package.

5.2 Low-speed approximation

In most cases of radar detection, the full relativity treatment is not needed. One of the goals of the thesis is therefore to build up a simplified package for small velocities.

As mentioned in chapter 2, the Special relativity models should approach the Galilean transformation in the limit of velocity small in comparison with the speed of light. This fact is further used to validate the results of the generic Matlab codes. The low-speed Matlab package only contains the Galilean transformation and non-relativistic Doppler shift. This considerably simplifies the evaluation.

The Galilean transform can be derived from the Lorentz transformation under the condition $\beta \rightarrow 0$. Applying this to explicit transformation in section 2.3, the fields remain unchanged under the Galilean transform

$$\mathbf{E} = \mathbf{E}', \mathbf{B} = \mathbf{B}'. \quad (5.7)$$

The transformation of the position four-vector simplifies to

$$\mathbf{r}' = \mathbf{r} + \mathbf{v}_0 \beta ct, \quad (5.8)$$

and the time coordinate remains the same in both frames

$$ct' = ct \quad (5.9)$$

This approximation will focus only on the frequency changes, the others are neglected. Therefore, neglecting the amplitude modulation of the fields under transformation to the moving frame, the above transformations of plane wave field lead to a well-known non-relativistic Doppler shift

$$\omega = \frac{\omega'}{1 - \beta \mathbf{n} \cdot \mathbf{v}_0}. \quad (5.10)$$

The propagation vector of the plane wave $\mathbf{n}' = \mathbf{n}$ remains unchanged.

In this approximation, the frequency shift (5.10) will be used even for general fields when they are observed far from their sources (far-field region). In the far-field region, the propagation direction \mathbf{n} will be represented with the difference unit vector \mathbf{R}_0 .

This far-field approximation will be used to evaluate scattered fields in the laboratory with further assumption that the difference vector remains constant through the observation time and with a sign change in the denominator of (5.10), i.e.,

$$\omega' = \frac{\omega}{1 + \beta \mathbf{R}_0 \cdot \mathbf{v}_0}. \quad (5.11)$$

The equations (5.10) and (5.11) are drawn as the left, and the right green block in flowchart 5.2.

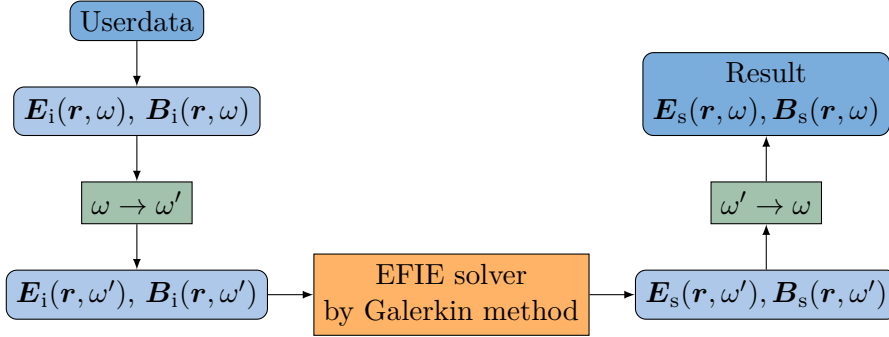


Figure 5.2: Approximation for low speed.

Chapter 6

Results

This chapter presents numerical examples resulting from the algorithms detailed in the previous two chapters 4 and 5. Throughout the chapter, firstly, the goal of the simulation is introduced, then the settings of the program are described, and last, the results are plotted and discussed. The main purpose of this chapter is to test every independent algorithm built in this thesis. For more information about each program, see the sections 4.2, 5.1, and 5.2.

For the sake of presentation, this chapter assumes illumination of the moving object with a plane wave of sinusoidal timecourse at frequency ω_0 , which is modulated in amplitude by Gaussian curve of width σ . Specifically, the frequency spectrum of the plane wave reads

$$\mathbf{E}_0(\omega) = \frac{1}{\sigma\sqrt{2\pi}} \left(e^{-\frac{1}{2}\left(\frac{\omega-\omega_0}{\sigma}\right)^2} + e^{-\frac{1}{2}\left(\frac{\omega+\omega_0}{\sigma}\right)^2} \right) \widetilde{\mathbf{E}}_0. \quad (6.1)$$

Particular values used for the subsequent calculations are $\omega_0 = 2\pi \cdot 10^9 \text{ s}^{-1}$ and $\sigma = 4\pi \cdot 10^8 \text{ s}^{-1}$ which roughly corresponds to short pulses radiated by a mono-pulse radar. Vector $\widetilde{\mathbf{E}}_0$ prescribes the overall amplitude and polarization of the plane wave, it is independent of frequency and changes in each example. Particular values of vector $\widetilde{\mathbf{E}}_0$ are shown in each example.

6.1 Electrically small perfectly conducting sphere

The first object of interest is an electrically small, perfectly conducting sphere because this scattering problem can be well approximated by polarizable a dipole particle and can be solved analytically as shown in the previous chapter 5.1. Hence, the analytical approach can validate the method of moments solution and, at the same time, the discrete full Lorentz transformation from section 4.2 since the numerical forms of both are not present in the dipole approximation.

6.1.1 Program settings

The dipole approximation assumes an ideal sphere, however, the Galerkin method has to use a triangularized “origami” model of a spherical surface. Two

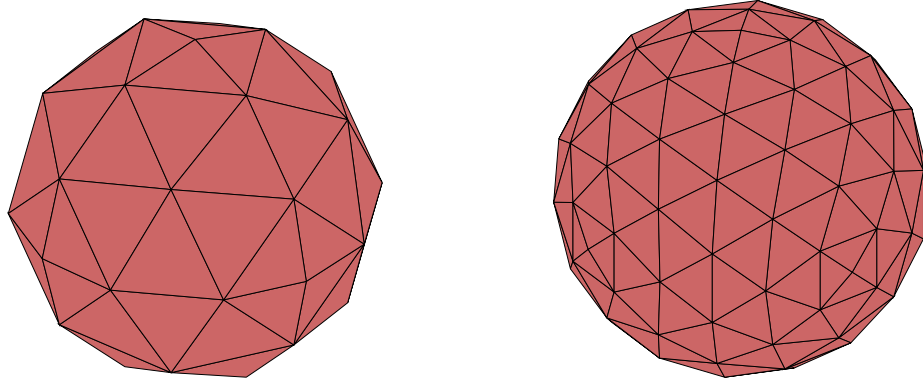


Figure 6.1: Discretized spherical surface consisting of 38 and 110 nodes.

discretizations, consisting of 38 and 110 nodes, were chosen. The geometrical accuracy of the used polyhedrons can be reviewed in figure 6.1.

Other settings are listed in table 6.1. In order to test the implementation thoroughly, the propagation vector \mathbf{n} and the field vector \mathbf{E}_0 were chosen randomly. If the approximation of sphere by dipole has to hold, the radius of the sphere a must be much less than wavelength λ_0 . Therefore, the author chose $a = 0.05\lambda_0/(2\pi) \approx 0.0785\lambda$.

Table 6.1: User input for the spherical setup

User input		
quantity	value	units
vector position \mathbf{r} of the observer in the laboratory	$\begin{pmatrix} 0 \\ -0.5 \\ 0 \end{pmatrix}$	[m]
vector position of the center of the sphere at time $t = 0$	$\begin{pmatrix} 0 \\ 0 \\ 0 \end{pmatrix}$	[m]
vector $\widetilde{\mathbf{E}}_0$	$\begin{pmatrix} 0.9649 \\ 0.1576 \\ -0.3707 \end{pmatrix}$	[V · m ⁻¹]
direction of velocity vector \mathbf{v}_0	$\begin{pmatrix} 1 \\ 0 \\ 0 \end{pmatrix}$	[-]
direction of plane wave propagation \mathbf{n}	$\begin{pmatrix} 0.2449 \\ 0.4809 \\ 0.8419 \end{pmatrix}$	[-]

■ 6.1.2 Results for $v = 10^{-3}c$ and $v = 0.8c$

Because the field was chosen randomly, only one component of $\widetilde{\mathbf{E}}_0$ will be plotted since the other two elements will not supplement any new information.

The left panels of figures 6.2 and 6.3 show the time course of the x -component of the scattered field \mathbf{E}_s at the observer's position. In the right panels of the figures, the magnitude of frequency spectrum $|E_{sx}|$ is plotted. Three different cases were considered, they consist of an analytical dipole approximation and two different discretizations which are evaluated with numerical routine.

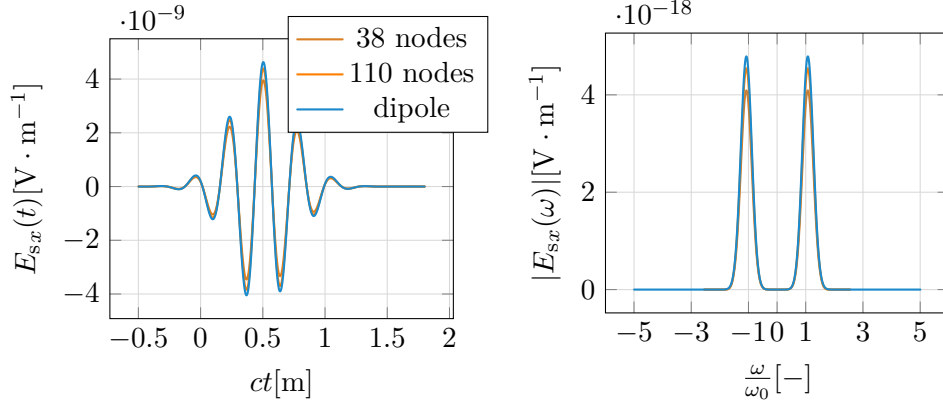


Figure 6.2: $E_{sx}(t)$ and $|E_{sx}(\omega)|$ of three different sphere descriptions for velocity $v = 10^{-3}c$

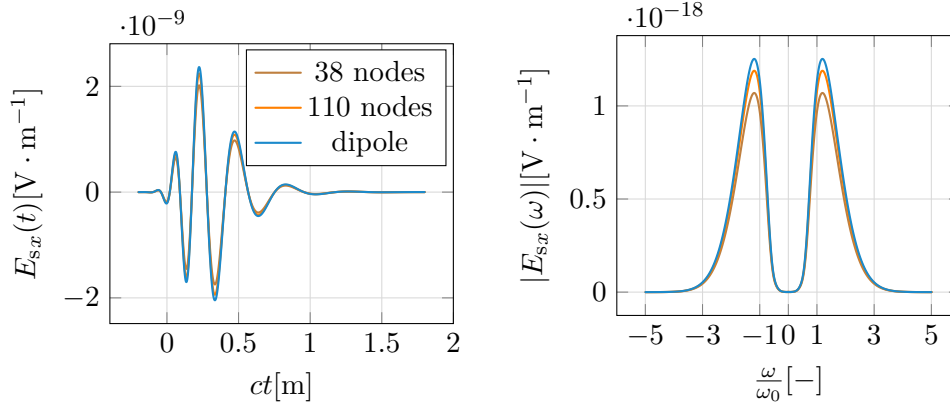


Figure 6.3: $E_{sx}(t)$ and $|E_{sx}(\omega)|$ of three different sphere descriptions for velocity $v = 0.8c$

As can be seen from both examples, the frequency is raising with increasing velocity, which results in squeezing the impulse in the time domain. Also for great velocities the frequency spectrum is stretching towards the higher frequencies.

Comparing the two examples it can be seen that overall the agreement is good with only slight and expected dependence on the discretization of the sphere. The trend can be clearly seen from the spectrum in figure 6.3 - the more nodes by which the sphere is approximated, the more precise results. Nevertheless, using more precise discretizations rapidly increases the computational time. Therefore, the quality of the results is mostly in the users' hands and it depends on how good the discretization of the object is

and how long can the calculations take. Despite this, the example clearly validates the numerical routine. Now, when the main code is validated, it turns the coat and will be used as a reference for validation of low-speed approximation from section 5.2.

6.2 Thin-strip dipole discretized by 72 nodes

In this chapter, a slightly more complex object will be used to see the validity and limits of the low-speed algorithm from section 5.2. The validated main algorithm now serves as a control tool. Concurrently, the abilities of the solver of the main solution from section 4.2 will be tested by using a different object - the thin-strip dipole moving along its length. Both algorithms will be executed for different velocity magnitudes and compared to each other to see the limits of low-speed approximation.

6.2.1 Program settings

The strip is discretized by a triangle mesh consisting of 72 nodes which can be seen in figure 6.4. The length of the strip was chosen to represent a macroscopical object as $l = 15$ cm. The width of the strip is $w = l/20 = 0.75$ cm.

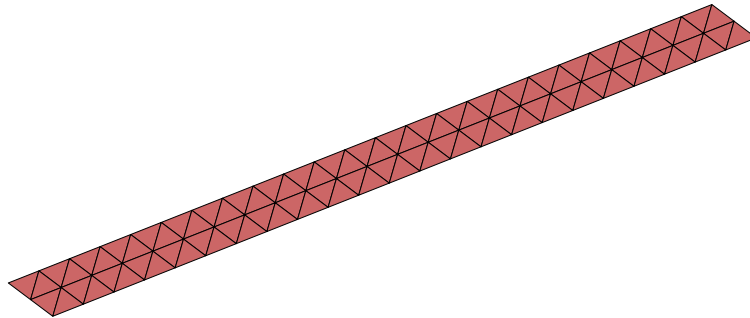


Figure 6.4: Mesh of a thin-strip dipole discretized by 72 nodes

The strip's length is rotated in the direction of the x -axis, which means it is moving in a longitudinal direction because the velocity vector \boldsymbol{v}_0 is also pointing in the direction of x as can be seen in table 6.2. The distance of the observer and the object at $t = 0$ was chosen 7.5 m since for bigger distances it was hard to fulfil the Nyquist condition for the low-speed approximation. The reason why has been left unknown to the author until finishing the thesis. The plane wave arrives in an orthogonal direction to the strip's motion, which should minimize the Doppler shift. Even if a bigger distance would be more suitable for the low-speed, far-field approximation, it still can give a satisfying outcome for small velocities since the travelled path during the observation time is negligible compared to the distance between the observer and the object. The vector $\widehat{\boldsymbol{E}}_0$ has been chosen arbitrarily.

Table 6.2: User input for the thin-strip dipole setup

User input		
quantity	value	units
vector position \mathbf{r} of the observer in the laboratory	$\begin{pmatrix} 0 \\ -7.5 \\ 0 \end{pmatrix}$	[m]
vector position of the center of the sphere at time $t = 0$	$\begin{pmatrix} 0 \\ 0 \\ 0 \end{pmatrix}$	[m]
vector $\widetilde{\mathbf{E}}_0$	$\begin{pmatrix} 1 \\ 6 \\ 0 \end{pmatrix}$	[V · m ⁻¹]
direction of velocity vector \mathbf{v}_0	$\begin{pmatrix} 1 \\ 0 \\ 0 \end{pmatrix}$	[–]
direction of plane wave propagation \mathbf{n}	$\begin{pmatrix} 0 \\ 0 \\ 1 \end{pmatrix}$	[–]

6.2.2 Results for $v = 10^{-6}c$, $v = 10^{-4}c$ and $v = 10^{-3}c$

In this example, the data are plotted only in the frequency domain because the low-speed algorithm focuses only on the frequency shift as was stated in section 5.2. The programs have been run over a variety of object's velocities to receive most of the information about the qualities of low-speed approximation. Then the author chose some exemplary cases to outline the tendency of the solution. Unfortunately, the unexplained modulation of amplitude occurred. Although some modulation was expected, the expectation was about maximal 1.2 scaling for smaller velocities. Until finishing this thesis, the reason, why the scaling difference is about 10^4 , still remains unknown. For this difference, the linear y -axis was useless, therefore the author decided to plot $|E_{sx}(\omega)|$ on the logarithmic y -axis as can be seen in the following figures in 6.5.

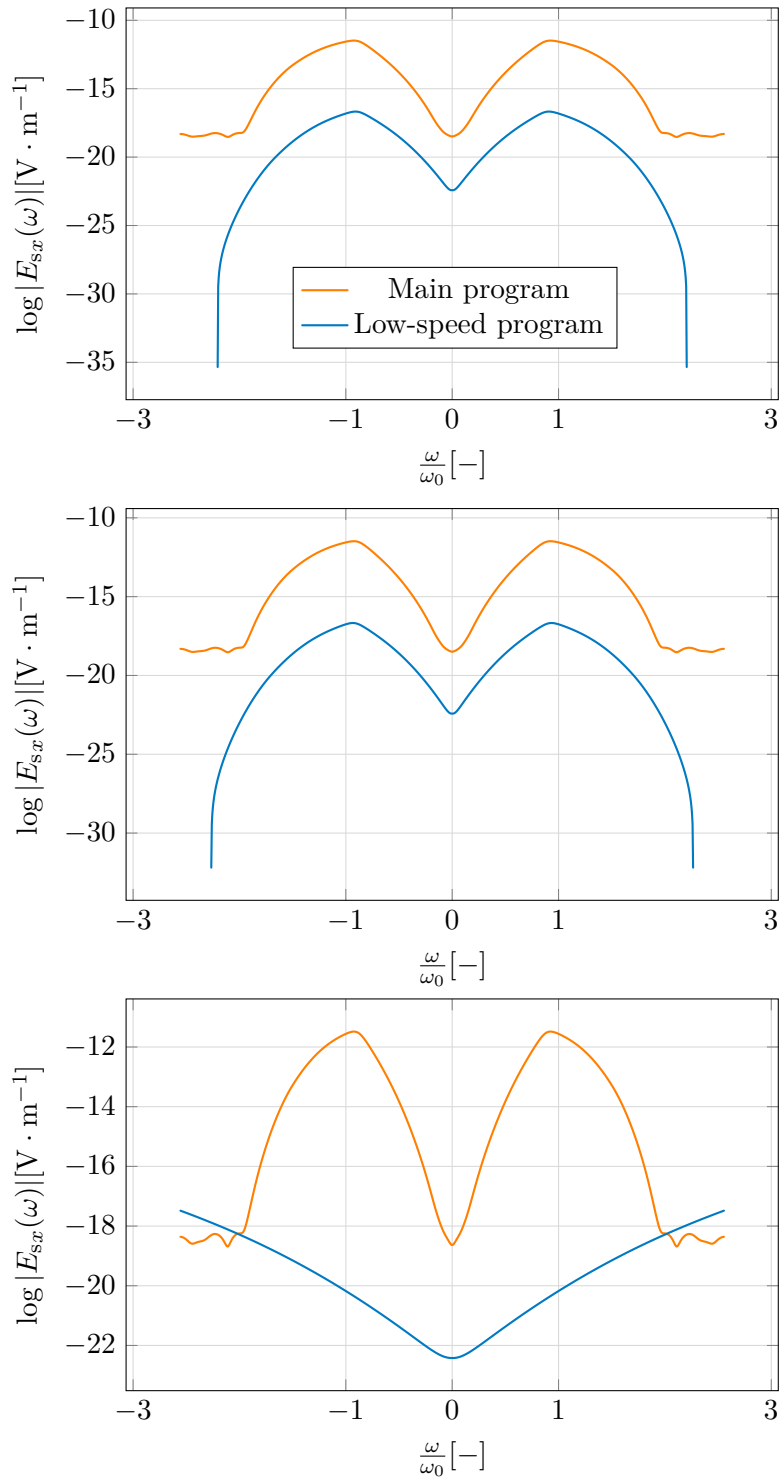


Figure 6.5: $\log |E_{sx}(\omega)|$ of the main and the low-speed program for velocity $10^{-6}c$, $10^{-4}c$ and $10^{-3}c$.


In the first figure in 6.5, for velocity $10^{-6}c$ can be seen that both algorithms provide, despite the aforementioned amplitude modulation, matching results.

It can be concluded that for these settings the approximation holds properly.

The second figure in 6.5 represents data for velocity $10^{-4}c$. There started some differences in frequency stretch to occur. It is notable, that the Main solver solution decreases in frequency spectrum a bit faster than the low-speed. This is caused by neglecting the Lorentz factor γ during the approximation, which led to equation (5.10). Still, the low-speed algorithm can be valid as a rough approximation, which can give the user quicker insight into the situation than the main code.

In the third figure in 6.5, the low-speed algorithm stops working properly and shows significant errors. The conclusion made from the other testing velocities is the following:

For this specific setup, the velocity above the edge, which is circa $2 \cdot 10^{-4}c$, the enormous error appears. Therefore the low-speed approximation should be used for much smaller velocities. The safe area is about velocity $10^{-6}c$, where approximated results hold with reality. For higher velocities between $10^{-5}c$ and $10^{-4}c$ can the program gives a quick overview of reality and the user has to call the main algorithm to obtain precise values. The low-speed algorithm provided to work in assumed speed interval, although unexplained amplitude modulations did occur.



Chapter 7

Conclusion

In summary, a brief introduction to the theory of special relativity was made. There were introduced the Lorentz transformation, the inertial frame equivalence and the frame-hopping technique which can significantly simplify the solution of the object's scattering. After gaining the ability to transform the observer in the co-moving frame, it was derived how the electric field integral equation will be numerically solved in the rest frame of the object, using the pre-implemented package operating with the Galerkin method. After the preparation of these tools, the possible solutions to the problem were outlined. The author discussed the strengths and weaknesses of every solution and prepared the main algorithm for solving the problem.

Apart from the main algorithm, two other particular solutions were built primarily for testing purposes. One consisted of limiting the problem only to a small sphere dipole, the other one assumed the object's velocity is much smaller than the speed of light.

After setting all the programs main package was tested. The main program package for scattering of an electromagnetic wave by a moving highly-conducting object has been proven to be successfully implemented, which means the essential goal of this thesis was solved.

The low-speed package was also implemented and proved to work, however, an unexpected amplitude modulation occurred. The author will try to figure out the singularity in further versions of the program.

The current limitations of the program are the need to use only the plane wave field as the source and the condition that the object was made from Perfect Electric Conductor (PEC). The second condition can be easily broken. For assuming different types of objects, the current PEC solver can be easily extracted and replaced by a different solver without changing any other part of the code.

The plane wave limitation was caused by the computational complexity of the found solution. The author assumes there is a faster way of calculating the problematic multiple IFFTs or a path to avoid using that approach at all. The possible solution could be similar to the *Goertzel algorithm*[20] and the *Cooley-Tukey FFT algorithm*[21]. The author is looking forward to getting acquainted with problematic of digital signal processing to find the solution. Sadly, his current knowledge of the signal processing field is not enough to

solve the problem.

The other way is to gain information about input sources through their description by dipole moments. The same output is received from the method of moments. Then, the transformation will be the same as in the subsection 4.1.4. This solution was not implemented because the author aimed to implement an algorithm for arbitrary source fields. This approach would require updating the current solver because parts of the plane wave field calculations are built-in into the solver in the current version of the program. Using the dipoles as the source approximation also would prevent the user from asking for the plane wave source since it is impossible to model an ideal plane wave by a finite number of dipoles, which may not be a problem since the plane wave is an ideal phenomenon which does not exist in reality.

One of the possible ways to improve or further develop programmed scripts in the future will be implementing them in the graphical user interface to make the software more user-friendly. The next stages of this project will include adjusting the codes to the form of a built-in add-on to the Matlab package[11] in the future.



Bibliography

- [1] Merrill I. Skolnik. *Introduction to radar systems*. McGraw Hill, 2001, p. 772. ISBN: 9780072881387.
- [2] “RADIO DETECTION AND RANGING”. In: *Nature* 152.3857 (Oct. 1943), pp. 391–392. DOI: 10.1038/152391b0.
- [3] Jan Vrba, Miroslav Lapeš, and Ladislav Oppl. “Technical aspects of microwave thermotherapy”. In: *Bioelectrochemistry and Bioenergetics* 48.2 (May 1999), pp. 305–309. DOI: 10.1016/s0302-4598(99)00039-2.
- [4] “Radar astronomy”. In: *Wikipedia* (May 2022). URL: https://en.wikipedia.org/wiki/Radar_astronomy.
- [5] Hugh D. Griffiths et al. *Stimson’s Introduction to Airborne Radar*. SciTech Publishing, Incorporated, 2014, p. 774. ISBN: 9781613530221.
- [6] “Parker Solar Probe”. In: *Wikipedia* (May 2022). URL: https://en.wikipedia.org/wiki/Parker_Solar_Probe.
- [7] B. L. Michielsen et al. “Three-dimensional relativistic scattering of electromagnetic waves by an object in uniform translational motion”. In: *Journal of Mathematical Physics* 22.11 (Nov. 1981), pp. 2716–2722. DOI: 10.1063/1.524853.
- [8] Robert C. Restrck. “Electromagnetic Scattering by a Moving Conducting Sphere”. In: *Radio Science* 3.12 (Dec. 1968), pp. 1144–1154. DOI: 10.1002/rds19683121144.
- [9] Kuisong Zheng et al. “Electromagnetic Properties of a Complex Pyramid-Shaped Target Moving at High Speed”. In: *IEEE Transactions on Antennas and Propagation* 66.12 (Dec. 2018), pp. 7472–7476. DOI: 10.1109/tap.2018.2872164.
- [10] Hongyun Deng, Gaobiao Xiao, and Guomin Liu. “An Efficient Method for Calculating the Doppler Spectrum of an Arbitrarily Shaped Object in Uniform Motion”. In: *IEEE Transactions on Antennas and Propagation* 70.11 (Nov. 2022), pp. 10894–10902. DOI: 10.1109/TAP.2022.3191188.
- [11] *Antenna toolbox for Matlab*. Solver package. CTU in Prague. May 2023. URL: <http://www.antennatoolbox.com>.

- [12] Jean Van Bladel. *Relativity and Engineering*. Springer Berlin Heidelberg, 1984. DOI: 10.1007/978-3-642-69198-0.
- [13] A. Einstein. “Zur Elektrodynamik bewegter Körper”. In: *Annalen der Physik* 322.10 (1905), pp. 891–921. DOI: 10.1002/andp.19053221004.
- [14] David Morin. *Introduction to Classical Mechanics. With Problems and Solutions*. Cambridge University Press, 2008, p. 738. ISBN: 9780521876223.
- [15] Hans Stephani. *Relativity. an introduction to special and general relativity*. Cambridge University Press, 2004, p. 396. ISBN: 0521811856.
- [16] Andrew Zangwill. *Modern electrodynamics*. Cambridge University Press, 2013, p. 977. ISBN: 9780521896979.
- [17] Roger F. Harrington. *Field computation by moment methods*. IEEE Press, 1993, p. 229. ISBN: 0780310144.
- [18] S. Rao, D. Wilton, and A. Glisson. “Electromagnetic scattering by surfaces of arbitrary shape”. In: *IEEE Transactions on Antennas and Propagation* 30.3 (May 1982), pp. 409–418. DOI: 10.1109/tap.1982.1142818.
- [19] Eric W. Hansen. *Fourier transforms principles and applications. principles and applications*. Wiley, 2014, p. 755. ISBN: 9781118479148.
- [20] Gerald Goertzel. “An Algorithm for the Evaluation of Finite Trigonometric Series”. In: *The American Mathematical Monthly* 65.1 (Jan. 1958), p. 34. DOI: 10.2307/2310304.
- [21] James W. Cooley and John W. Tukey. “An algorithm for the machine calculation of complex Fourier series”. In: *Mathematics of Computation* 19.90 (1965), pp. 297–301. DOI: 10.1090/s0025-5718-1965-0178586-1.